ISPRS Journal of Photogrammetry and Remote Sensing 106 (2015) 157–171

Contents lists available at ScienceDirect

ISPRS Journal of Photogrammetry and Remote Sensing

journal homepage: www.elsevier.com/locate/isprsjprs

Mapping paddy rice planting areas through time series analysis of MODIS land surface temperature and vegetation index data

Geli Zhang [a], Xiangming Xiao [a,b,*], Jinwei Dong [a], Weili Kou [a,c], Cui Jin [a], Yuanwei Qin [a], Yuting Zhou [a], Jie Wang [a], Michael Angelo Menarguez [a], Chandrashekhar Biradar [d]

[a] Department of Microbiology and Plant Biology, and Center for Spatial Analysis, University of Oklahoma, Norman, OK 73019, USA
[b] Institute of Biodiversity Science, Fudan University, Shanghai 200433, China
[c] Department of Computer and Information Science, Southwest Forestry University, Kunming, Yunnan 650224, China
[d] International Center for Agricultural Research in Dry Areas, Amman 11195, Jordan

ARTICLE INFO

Article history:
Received 21 January 2015
Received in revised form 26 May 2015
Accepted 27 May 2015

Keywords:
Paddy rice fields
MODIS images
Land Surface Water Index (LSWI)
Enhanced Vegetation Index (EVI)
Land Surface Temperature (LST)
Flooding
Northeastern China

ABSTRACT

Knowledge of the area and spatial distribution of paddy rice is important for assessment of food security, management of water resources, and estimation of greenhouse gas (methane) emissions. Paddy rice agriculture has expanded rapidly in northeastern China in the last decade, but there are no updated maps of paddy rice fields in the region. Existing algorithms for identifying paddy rice fields are based on the unique physical features of paddy rice during the flooding and transplanting phases and use vegetation indices that are sensitive to the dynamics of the canopy and surface water content. However, the flooding phenomena in high latitude area could also be from spring snowmelt flooding. We used land surface temperature (LST) data from the Moderate Resolution Imaging Spectroradiometer (MODIS) sensor to determine the temporal window of flooding and rice transplantation over a year to improve the existing phenology-based approach. Other land cover types (e.g., evergreen vegetation, permanent water bodies, and sparse vegetation) with potential influences on paddy rice identification were removed (masked out) due to their different temporal profiles. The accuracy assessment using high-resolution images showed that the resultant MODIS-derived paddy rice map of northeastern China in 2010 had a high accuracy (producer and user accuracies of 92% and 96%, respectively). The MODIS-based map also had a comparable accuracy to the 2010 Landsat-based National Land Cover Dataset (NLCD) of China in terms of both area and spatial pattern. This study demonstrated that our improved algorithm by using both thermal and optical MODIS data, provides a robust, simple and automated approach to identify and map paddy rice fields in temperate and cold temperate zones, the northern frontier of rice planting.

1. Introduction

Rice is a major staple food for almost 50% of the world's population (Kuenzer and Knauer, 2013), and paddy rice fields account for more than 12% of the global cropland area (FAOSTAT, 2010). Asia has the largest paddy rice fields (Maclean and Hettel, 2002), and produced more than 90% of the rice in the world in 2011 (Kuenzer and Knauer, 2013). Global emissions of rice-based methane total 21–30 teragrams per year (Sass and Cicerone, 2002) and account for more than 10% of the total methane flux in the atmosphere (Ehhalt et al., 2001). Irrigation for agriculture consumes approximately 70% of the global fresh water withdrawals (Samad et al., 1992), and approximately one-quarter to one-third of the developed freshwater resources in the world are used for paddy rice irrigation (Bouman, 2009). The high water demands of irrigated agriculture have raised concerns about improving water resource management, including water conservation and water quality protection (Kuenzer and Knauer, 2013). Water management for paddy rice fields also affects methane emissions (Sass et al., 1999). Recently, paddy rice fields are recognized as a key risk factor for transmission of highly pathogenic avian influenza A (H5N1) virus (Gilbert et al., 2014; Gilbert et al., 2008), as paddy rice fields are an important habitat for free-ranging ducks and wild waterfowl in winter where the avian influenza virus may be transmitted. Therefore, it is important to

* Corresponding author at: Department of Microbiology and Plant Biology, and Center for Spatial Analysis, University of Oklahoma, Norman, OK 73019, USA. Tel.: +1 (405) 325 8941; fax: +1 (405) 325 3442.
E-mail address: xiangming.xiao@ou.edu (X. Xiao).

http://dx.doi.org/10.1016/j.isprsjprs.2015.05.011
0924-2716/

monitor and map paddy rice fields at regional and global scales in an effort to enhance our knowledge of food security, greenhouse gas emissions, water resource management, and transmission of infectious diseases.

Satellite remote sensing is recognized as a viable tool to map paddy rice fields, based on either optical or synthetic aperture radar (SAR) images. Although SAR data are not impacted by clouds or solar illumination, the SAR-based approach has not been used for large-scale paddy rice mapping due to limited data availability (Bouvet et al., 2009; Dong et al., 2006; Miyaoka et al., 2013; Wu et al., 2011; Yang et al., 2008). Many studies have used one to several optical images (e.g., Landsat) to map paddy rice at local scales with supervised or unsupervised classification methods (Li et al., 2012; Yoshikawa and Shiozawa, 2006). Optical sensors with high temporal resolutions (daily revisits) such as the Advanced Very High Resolution Radiometer (AVHRR), Système Pour l'Observation de la Terre (SPOT) (Kamthonkiat et al., 2005; Thi et al., 2012), and Moderate Resolution Imaging Spectrora diometer (MODIS), have also been used to map paddy rice fields at regional scales, based on the temporal characteristics of paddy rice fields (Chen et al., 2012; Gumma et al., 2011; Nuarsa et al., 2012; Peng et al., 2011; Son et al., 2013; Xiao et al., 2006, 2002b, 2005).

Rice is grown in flooded soils, and paddy fields are a mixture of open water and green rice plants during the early part of the growing season (transplanting phase). These characteristics can be readily identified using temporal profiles of vegetation indices such as the Land Surface Water Index (LSWI), Normalized Difference Vegetation Index (NDVI) and Enhanced Vegetation Index (EVI). Spectral signature analysis has shown that the LSWI values can temporarily be greater than the NDVI or EVI values during the flooding and transplanting phases (Xiao et al., 2006, 2002b, 2005). Based on this unique feature of paddy rice fields during the early period of the growing season, we developed an algorithm to identify and track the image pixels that were flooded and transplanted with seedlings over time (Xiao et al., 2006, 2005). The algorithm was used to map paddy rice at regional scales in southern China, South Asia, and Southeast Asia, where the air temperature stayed above 0 °C for most of the year and there is little or no snow cover, using an 8-day MODIS dataset in 2002 (Xiao et al., 2006, 2005).

Paddy rice has an expansion trend in mid- and high-latitude regions, such as northeastern China, where paddy rice croplands have rapidly expanded in the last decade. According to statistical data, the area of paddy rice fields in this region increased from 2.57×10^4 km^2 in 2000 to 4.33×10^4 km^2 in 2010, which represents an increase of approximately 68%. By 2010, paddy rice fields in the region accounted for more than 10% of the total rice agricultural area in China. As a result of this rapid growth, northeastern China has become a major food production region in China (Liu et al., 2013). The expansion of paddy rice could raise several environmental issues regarding water resources, soil erosion, bird habitats, and biodiversity because most paddy rice fields were converted from natural wetlands or land that was previously used to grow upland crops. Information and geospatial data about the area and spatial patterns of paddy rice agriculture in northeastern China is urgently needed because there is limited knowledge about their current distributions in this high-latitude region.

Direct application of the MODIS-based algorithms (Xiao et al., 2006, 2005) in temperate zones is likely to be complicated by snow and ice cover during the long winter season, by snowmelt in spring, and by the short plant growing season; and it is necessary to precisely identify the time period of the flooding and transplanting phases. Several previous studies have attempted to define the flooding and transplanting periods based on rice growth calendar data (such as the transplanting period) from agricultural meteorological stations (Peng, 2009; Peng et al., 2011; Shi et al., 2013; Sun et al., 2009). The rice growth calendar data were available from scattered agricultural meteorological stations, but there were large uncertainties when the station data were interpolated to regional or national scales. In addition, this station-based approach cannot be used for regions that have no agricultural meteorological stations. The determination of the transplanting phase is needed for the paddy rice mapping in the high latitude area where limited efforts have been made.

The objective of this study is twofold: (1) to develop an improved algorithm that combines land surface temperature (LST) and vegetation indices from MODIS sensors to map paddy rice fields in temperate and cold temperate zones, and (2) to quantify the area and spatial distribution of paddy rice agriculture in northeastern China in 2010 through the use of the improved algorithms and MODIS data in 2010. To achieve these goals, we first used MODIS-based land surface temperature data at a 1-km spatial resolution to determine the period that is suitable for flooding and rice plant transplanting over the course of a year for individual pixels. We then used vegetation indices to identify the pixels that contained a mixture of green rice plants and surface water within that period. The resultant paddy rice map at a 500-m spatial resolution was validated with samples from the very high resolution imagery in Google Earth and compared with the Landsat-based National Land Cover Dataset (NLCD) (Liu et al., 2014) and agricultural statistical data in 2010. This improved algorithm (robust, simple, and automated) will contribute to our future efforts to generate annual paddy rice maps and provide more accurate and updated data for studies of food security, water management, greenhouse gas emissions, and disease transmission.

2. Materials and methods

2.1. Study area

Northeastern China is composed of Heilongjiang, Jilin, and Liaoning Provinces (Fig. 1). It is located in a transition area between mountains and plains with an average elevation greater than 400 m (Fig. 1). The Lesser Khingan Mountain Range is located to the north and extends from the northwest to the southeast, and the Changbai Mountains are located on the southeast and extend from northeast to southwest. The plains are mainly located in the northeastern, western, and southern parts of the region and include the Sanjiang Plain, Songnen Plain, and Liaohe Plain. The river system is large and extensively distributed in the northeastern region, including the Heilongjiang River, Wusuli River, Songhua River, Nen River, and Liao River. The region has cold temperate and humid/sub-humid climate. The average annual precipitation is approximately 500–800 mm, which mostly falls in July and August. The annual accumulated air temperature above 0 °C ranges from 2000 to 4200 °C d, and the annual accumulated air temperature above 10 °C ranges from 1600 to 3600 °C d. The number of frost-free days varies between 140 d and 170 d. Due to temperature limit, there is only one crop system in this region.

This region is an important area of agricultural production in China; according to the National Land Cover Dataset (Liu et al., 2014), it had a total cropland area of 29.97×10^4 km^2 in 2010 (Table 1), which accounted for 16.8% of the total cropland area in the country. The main crop species include soybean, corn, wheat, and paddy rice. Paddy rice accounted for 15.5% of the cropland in this region in 2010, and the region provided 10.2% of the paddy rice yield in China (Table 1) (Liu et al., 2014). The paddy rice fields are mainly distributed in the plain areas along the rivers.

2.2. MODIS data and preprocessing

The MODIS Land Science Team provides an 8-day composite MODIS Surface Reflectance Product (MOD09A1) at 500-m

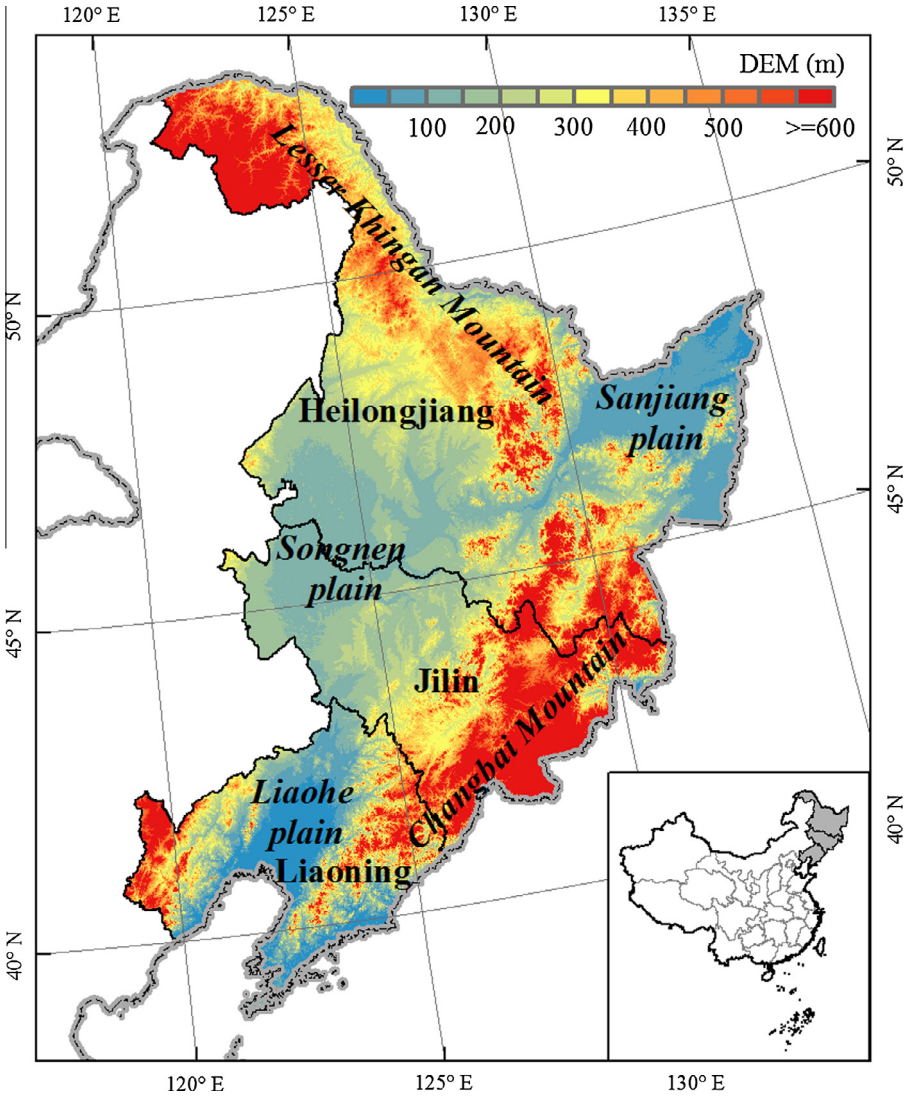

Fig. 1. Digital elevation model (DEM) of northeastern China. The study area covers three provinces in northeastern China.

Table 1
Summary of land area, paddy rice agriculture, and upland cropland from the Natural Land Cover Dataset (NLCD) in 2010 for the three provincial administrative units in northeastern China.

Province	Land area (km^2)	Area of upland cropland (km^2)	Area of paddy rice (km^2)	Percent of rice area with >=20% fractional cover in 1-km pixels (%)	Median percent of paddy rice within 1-km pixels (%)
Heilongjiang	452,782	135,645	26,701	95	42
Jilin	190,872	64,975	10,534	89	24
Liaoning	145,558	52,597	9237	93	32
Total	789,212	253,218	46,471	93	34

resolution (Vermote and Vermeulen, 1999). It includes seven bands: bands 1 (red: 620–670 nm), 2 (near infrared 1: 841–876 nm), 3 (blue: 459–479 nm), 4 (green: 545–565 nm), 5 (near infrared 2: 1230–1250 nm), 6 (shortwave infrared 1: 1628–1652 nm), and 7 (shortwave infrared 2: 2105–2155 nm). Standard MODIS products are organized in a tile system using a sinusoidal projection, and each tile covers an area of 1200 km × 1200 km (approximately 10° latitude by 10° longitude at the equator).

Northeastern China is covered by five tiles (H25V03, H26V03, H26V04, H27V04 and H27V05) of MOD09A1 data. We downloaded the five tiles for 2010 (46 composites per year) from the USGS EROS Data Center (https://lpdaac.usgs.gov/). Our MODIS preprocessing procedure included three components: (1) identifying clouds and cloud shadows, (2) calculation of spectral indices, and (3) gap-filling of vegetation indices.

We identified cloud cover and cloud shadows in two steps. First, we used the data quality information (the quality control flag layer) in the MOD09A1 products to extract the clouds and cloud shadows from each image. Second, we applied an additional restriction in which pixels with a blue reflectance of $\geqslant 0.2$ were also labeled as cloudy (Xiao et al., 2006, 2005) (round symbols in the LSWI curves in Figs. 2b and 3). Therefore, 46 maps of cloud and cloud shadow covers were generated. For each pixel, any 8-day composite that was identified as cloud and cloud shadow covers was excluded and gap-filled for further analyses.

The individual spectral bands in each of the 8-day composite surface reflectance MOD09A1 datasets were used to calculate four spectral indices: (1) NDVI, (2) EVI, (3) LSWI, and (4) normalized difference snow index (NDSI). Both NDVI and EVI are related to the vegetation canopy. NDVI has a saturation issue when it is used for closed canopies, and it is also sensitive to atmospheric

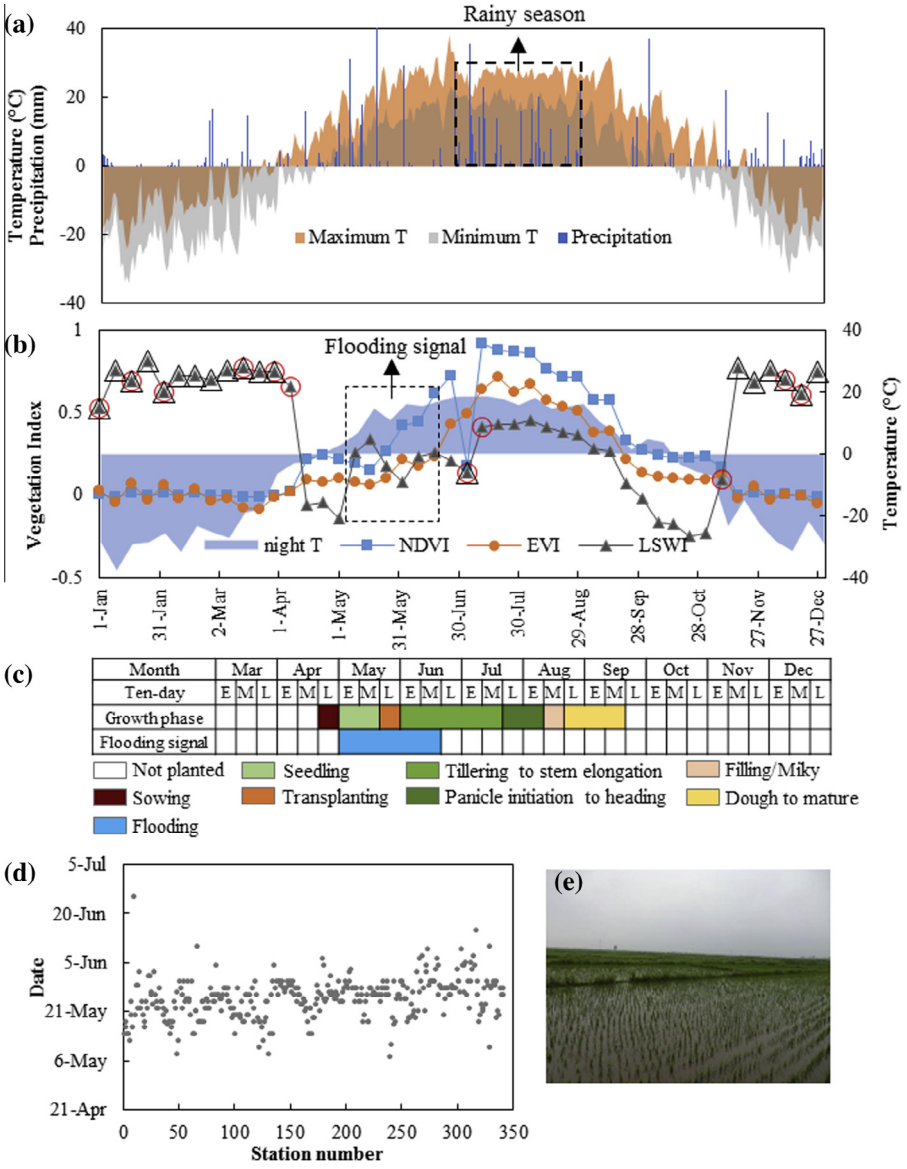

Fig. 2. (a) The annual variations of daily maximum temperature, daily minimum temperature, and daily precipitation in 2010 using one agricultural meteorological site as an example (Hulin site: 132.97°E, 45.77°N); (b) The seasonal dynamics of the Normalized Difference Vegetation Index (NDVI), Enhanced Vegetation Index (EVI), Land Surface Water Index (LSWI) and the MODIS-based nighttime land surface temperature from a paddy rice point in 2010 (132.825°E, 45.737°N); (c) the calendar for paddy rice growing systems in 2010 at the Hulin station based on the agricultural phenological observations data; (d) the calendar of flooding and transplanting for paddy rice for all the sites in the study area based on the MODIS LST data; (e) the picture of flooding and transplanting in a continuous paddy rice point. The hollow triangular and round symbols in (b) mean the cloud and cloud shadow from the MODIS quality layer and blue band >= 0.2, respectively, which are labeled on the LSWI curves.

conditions and soil background (Huete et al., 2002; Xiao et al., 2003b). EVI takes residual atmospheric contamination and variable soil and canopy background reflectance into account (Huete et al., 2002, 1997) because the blue band is sensitive to atmospheric conditions. LSWI was shown to be sensitive to equivalent water thickness (EWT; g H_2O/m^2) (Maki et al., 2004; Xiao et al., 2002a,b) because the SWIR band is sensitive to leaf water and soil moisture. NDSI is widely used for snow detection (Hall et al., 1995, 2002).

Bad-quality observations (clouds and cloud shadows) in time series vegetation indices need to be gap-filled. When the continuous gaps contained no more than three consecutive points, the linear interpolation approach was used to gap-fill the time series data. More than three consecutive missing observations were limited in our study area (temperate zone) as the effects of clouds and clouds shadows in the growing season are much less than in tropical regions. While snow effects are severe in winter, we just set the bad observations as no-data since it is out of the growing season. We did not interpolate bad-quality observations if they occurred during the first or last 8-day composite periods in a year.

The MODIS Land Science Team provides 8-day composite MODIS land surface temperature products at 1-km resolution, such as MOD11A2 (from the Terra satellite) and MYD11A2 (from the Aqua satellite). The LST data include daytime (local time ~10:30 AM from Terra and ~13:30 PM from Aqua) and nighttime (~22:30 PM from Terra and ~01:30 AM from Aqua) temperature observations. Due to remarkable daily temperature variation in the high latitude areas, frost status and crop planting are determined by daily minimum temperature. Thus, we used the nighttime temperature from MYD11A2 in 2010 to define the thermal growing season (Linderholm et al., 2008) and the starting time window of the flooding and rice transplanting; specifically, the starting date of stable temperatures above 0, 5 and 10 °C (Fig. 4) were calculated. The digital number values (DN) from MYD11A2 were converted to LST with centigrade unit values based on the

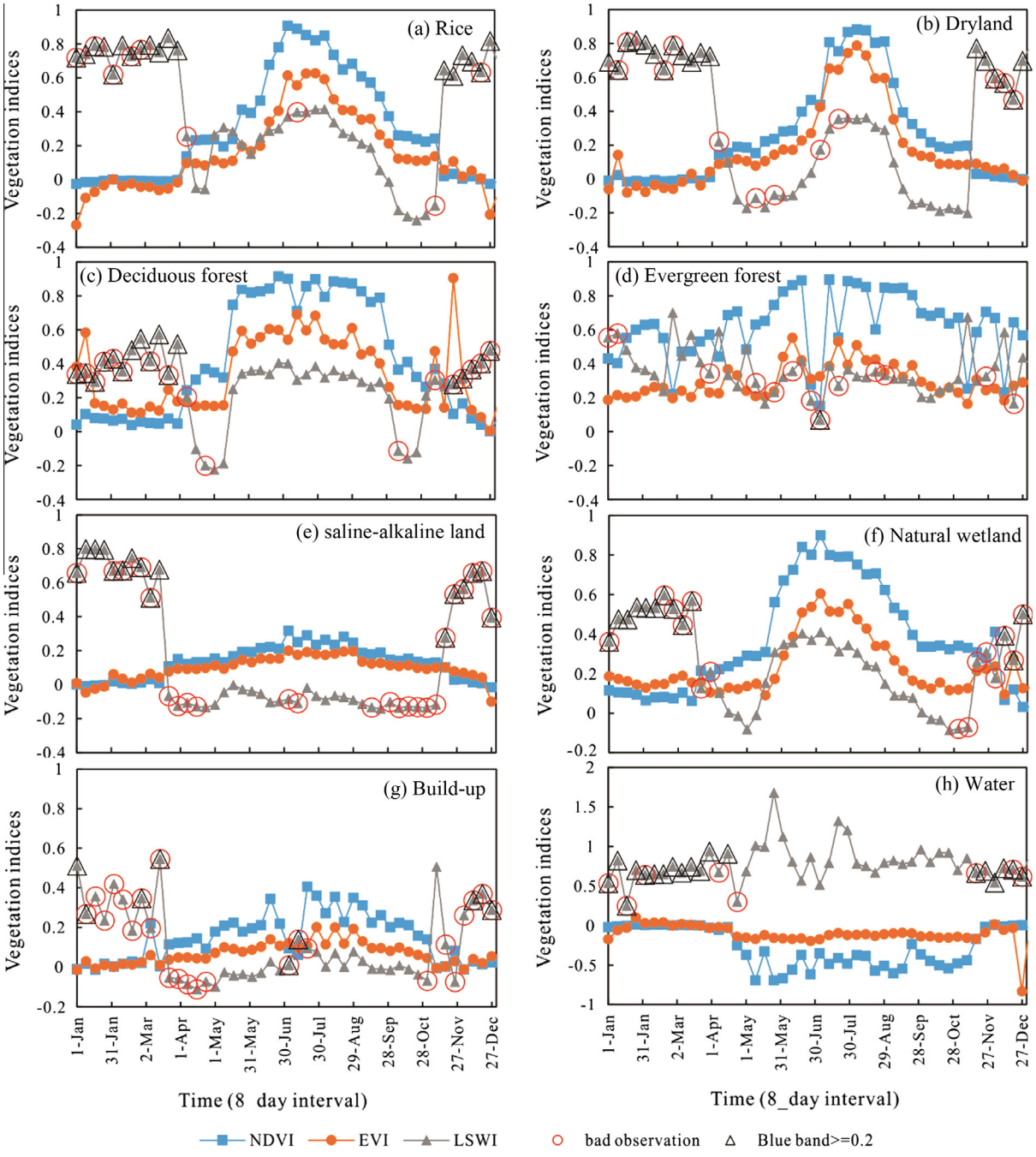

Fig. 3. The seasonal dynamics of the Normalized Difference Vegetation Index (NDVI), Enhanced Vegetation Index (EVI), and Land Surface Water Index (LSWI) of (a) paddy rice (47.836°N, 133.179°E), (b) dryland (upland crop, 47.553°N, 130.655°E), (c) deciduous forest (48.358°N, 134.359°E), (d) evergreen forest (43.886°N, 125.293°E), (e) saline-alkaline land (45.856°N, 124.724°E), (f) natural wetland (47.210°N, 124.458°E), (g) build-up (43.886°N, 125.293°E), and (h) water (45.236°N, 124.297°E) in 2010. The hollow triangular and round symbols mean the cloud and cloud shadow from the MODIS quality layer and blue band >= 0.2, respectively, which are labeled on the LSWI curves.

following formula: LST (°C) = DN × 0.02–273.15 (Wan, 2008; Wan et al., 2002). The LST data with bad observations in a time series were also gap-filled using the linear interpolation approach (Pan et al., 2015). The resultant maps of the starting date of stable temperatures above 0, 5 and 10 °C were resampled to 500 m using the nearest neighbor method to be spatially consistent with the vegetation index maps from MOD09A1.

2.3. Algorithms to identify inundation and paddy rice fields

The temporal dynamics of paddy rice fields can be characterized by three phases: (1) flooding and rice transplanting, (2) rapid plant growth and canopy closure after transplanting, and (3) the fallow period after the rice harvest (LeToan et al., 1997). These three phases are illustrated in Fig. 2. In the first phase, the land surface is covered by a mix of paddy rice plants and water, as observed by sensors and people (Xiao et al., 2002c) (Fig. 2e). In the second phase, the rice canopy covers most of the surface area approximately 50–60 d after transplanting (Xiao et al., 2006, 2005), and sensors and people can only see rice canopy. At the end of the growth period prior to harvesting (the ripening stage), the rice canopy has lower leaf and stem moisture contents and more senescent leaves (Xiao et al., 2006, 2005) (Fig. 2). In the third phase, the land surface is a mixture of rice plant residuals and soil.

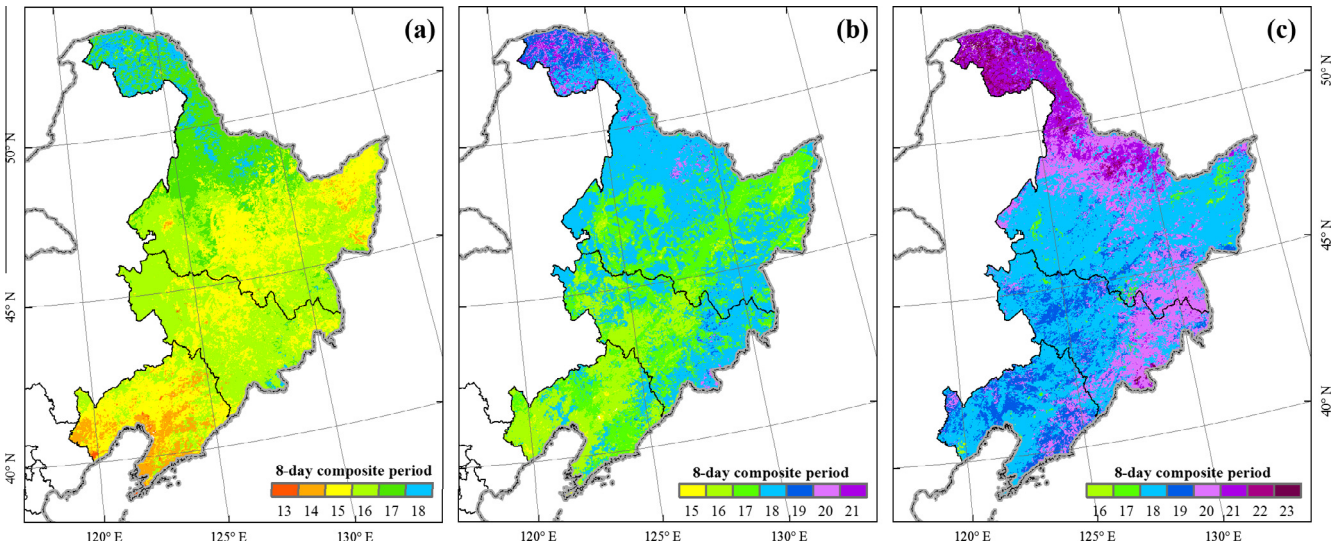

Fig. 4. Spatial distributions of the starting dates of nighttime land surface temperature (LST) remaining stable above (a) 0 °C, (b) 5 °C, and (c) 10 °C in northeastern China based on MODIS LST data in 2010.

Our previous studies presented a phenology-based algorithm to identify and map paddy rice in southern China and Southeast Asia (Xiao et al., 2006, 2005). The algorithm captures the characteristics of flooding signals and rapid plant growth from the period of flooding/transplanting to the period with a full canopy. When the paddy rice fields are flooded and transplanted, there is a temporary inversion of the vegetation indices in which the LSWI values either approach or exceed the NDVI or EVI values (Fig. 2b); this can be characterized as the flooding/transplanting signal in paddy rice fields (Xiao et al., 2002b). For the 500-m spatial resolution MODIS images, we slightly relaxed the threshold and used a confidence interval of 5% to identify a flooded/transplanted pixel: LSWI + 0.05 ⩾ EVI or LSWI + 0.05 ⩾ NDVI (Xiao et al., 2006, 2005). The flooding and transplanting areas in each 8-day composite in one year were identified as potential areas for paddy rice fields. Second, our previous studies also showed that rice crops grow rapidly after transplanting, and the LAI usually reaches its peak in approximately two months in southern China and Southeast Asia (Xiao et al., 2006, 2005, 2002c). The EVI value of a rice pixel reaches half of the maximum EVI value (in that crop cycle) within five 8-day increments (approximately 40 d) after transplanting.

In observations with snow cover (winter season) and/or snowmelt (early spring season), the LSWI values are often higher than the EVI values (Fig. 2b), which affect the algorithm described above (Fig. S1). Here, we propose an improved mapping procedure that consists of two steps: (1) use land surface temperature to define a suitable period of flooding and rice transplanting in a year for individual pixels, and (2) use vegetation indices to identify the signal of flooding and transplanting within the suitable period of flooding and rice transplanting.

Rice plant transplanting occurs when a stable temperature threshold is reached, so the plants will not suffer damage from cold temperatures. By comparing the observational agricultural phenology data and the temporal profile of nighttime LST (Fig. 2), we determined that the likely starting date of flooding and transplanting (SOF) is when the nighttime LST remains above 5 °C (LST 5 °C for short). Because snowmelt occurs after the nighttime LST is above 0 °C, no snow cover will exist after the nighttime LST > 5 °C. Moreover, we found that the flood/open-canopy signals of paddy rice fields mainly occur before the dates that the LSWI and EVI curves cross (Figs. 2 and 3), where the EVI value is equal to approximately 0.35 (EVI 0.35 for short) during the early part of the growing season of paddy rice. The period of EVI 0.35 corresponds to the end of the flood (EOF) and the open canopy stage in the rice fields. Therefore, we set the EVI 0.35 point as the EOF.

We then used the EVI and LSWI data within the suitable period for flooding and transplanting to identify the observations with signals of flooding and transplanting (Eq. (1)) and assumed a pixel to be a "potential or likely" paddy rice field if one or more observations were identified in that manner (Eq. (2), Fig. 5).

$$F_{Ti} = \begin{cases} 1 & (LSWI_{Ti} + 0.05 \geqslant EVI_{Ti}) \\ 0 & (LSWI_{Ti} + 0.05 < EVI_{Ti}) \end{cases} \quad (1)$$

where T_i is the 8-day composite period between the SOF and EOF.

$$Rice_p = \sum (F_{T1}, F_{T2,\cdots,F_{Tn}}) \quad (SOF \leqslant T \leqslant EOF) \quad (2)$$

where $Rice_p$ is the potential paddy rice area, and F_T is the flooding area in the 8-day composite at T between the SOF and EOF.

2.4. Regional implementation of the paddy rice mapping algorithm

It is challenging to implement our algorithm to map paddy rice fields at a regional scale because several factors (e.g., snow cover, water bodies, and other vegetated land-cover types) may cause classification error of commission. In our previous studies, several algorithms were used to generate various masks (snow, permanent water, evergreen vegetation) at regional scales, which reduce the commission error in detecting paddy rice fields (Xiao et al., 2006, 2005). In this study, we added four new masks to improve the accuracy of the MODIS-based paddy rice mapping: (1) mixed pixels with water and natural vegetation, (2) sparse vegetation, (3) natural deciduous vegetation, and (4) natural wetlands (Fig. 6).

2.4.1. Snow cover

We used the algorithm developed for the MODIS snow product to generate snow cover masks, which is based on the NDSI and NIR bands (Hall et al., 1995, 2002). The pixels with the thresholds NDSI > 0.40 and NIR > 0.11 were labeled as snow cover in this study. Forty-six maps of snow cover were generated. The observations that were identified as snow cover were excluded from the identification of paddy rice fields.

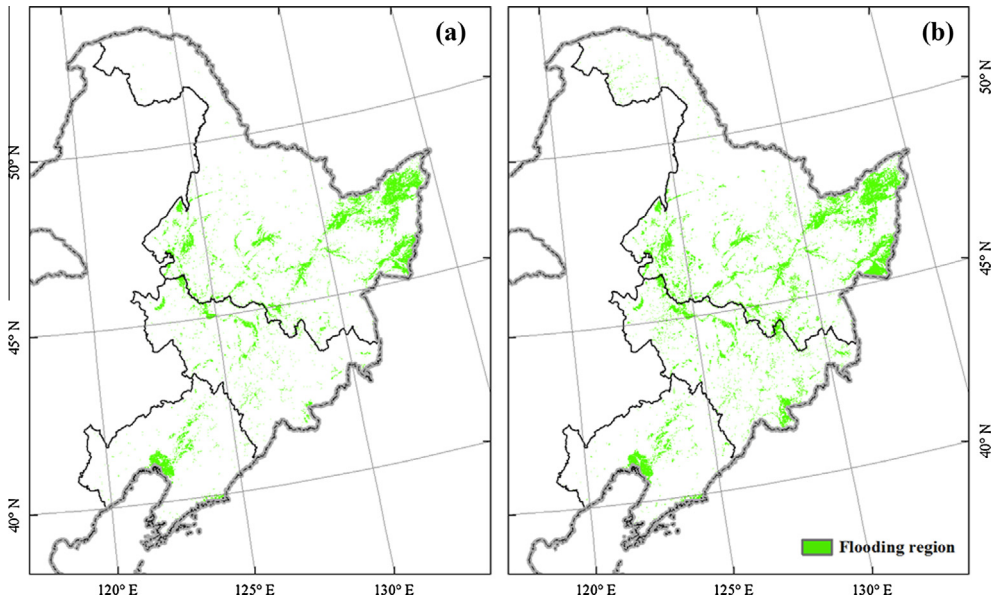

Fig. 5. Spatial distribution of flooding/transplanting pixels in northeastern China in 2010, based on (a) flooded/transplanted pixels during the period from the starting date of LST 5 °C to the date of EVI = 0.35, and (b) flooded/transplanted pixels during the period from May to June (from 16th to 23rd 8-day MODIS composites).

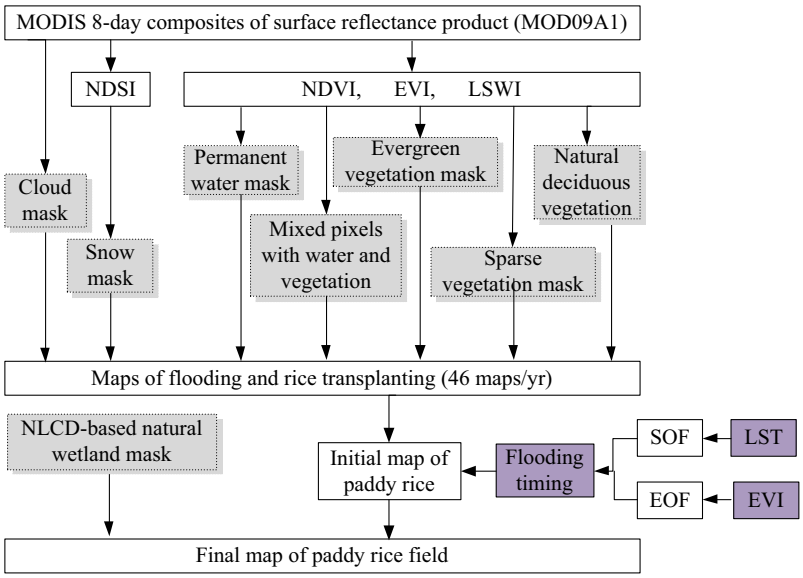

Fig. 6. A schematic diagram illustrating the algorithms for large scale mapping of flooding and paddy rice fields from MODIS 8-day surface reflectance images at 500-m spatial resolution and MODIS 8-day land surface temperature data at 1-km spatial resolution. One year of 8-day MODIS surface reflectance data (a total of forty-six 8-day composites) and thermal data (a total of forty-six 8-day composites) are used as input data.

2.4.2. Persistent water bodies

We analyzed the seasonal NDVI and LSWI profiles of water bodies for the year, and an observation was assumed to be a water body if NDVI < 0.1 and LSWI > NDVI. For each pixel, we counted the number of 8-day periods identified as a water body in the year (46 images). Pixels were identified as a persistent water body if it was labeled as a water body in ten or more 8-day composite periods during the year (Fig. 3h). The resultant mask of persistent water bodies is shown in Fig. 7a. The pixels identified as persistent water bodies were excluded in the identification of paddy rice fields.

2.4.3. Mixed pixels with natural vegetation and water bodies (edge pixels of rivers and lakes)

Many mixed pixels of natural vegetation (grass, shrub or trees) and water are located near rivers, lakes, and saline and alkaline areas. These mixed pixels often have higher LSWI values than EVI values throughout the plant growing season. During the rainy season in the summer (Fig. 2a), precipitation enhances the flooding signal for these pixels, while paddy rice fields have high vegetation coverage and no flooding signals. Therefore, the flooding areas in the summer can be used to extract the mixed vegetation/water pixels. We generated the flooding maps using the 26–30th MODIS 8-day composites (i.e., from 20 July to 21 August) using the formula LSWI + 0.05 ⩾ EVI and then merged them into one mask of mixed vegetation and water pixels (Fig. 7b).

2.4.4. Evergreen vegetation

Croplands and other deciduous vegetation usually had negative LSWI values in several 8-day periods due to exposed soils and/or senescent vegetation, but evergreen vegetation types (with green vegetation throughout the year) always had positive LSWI values

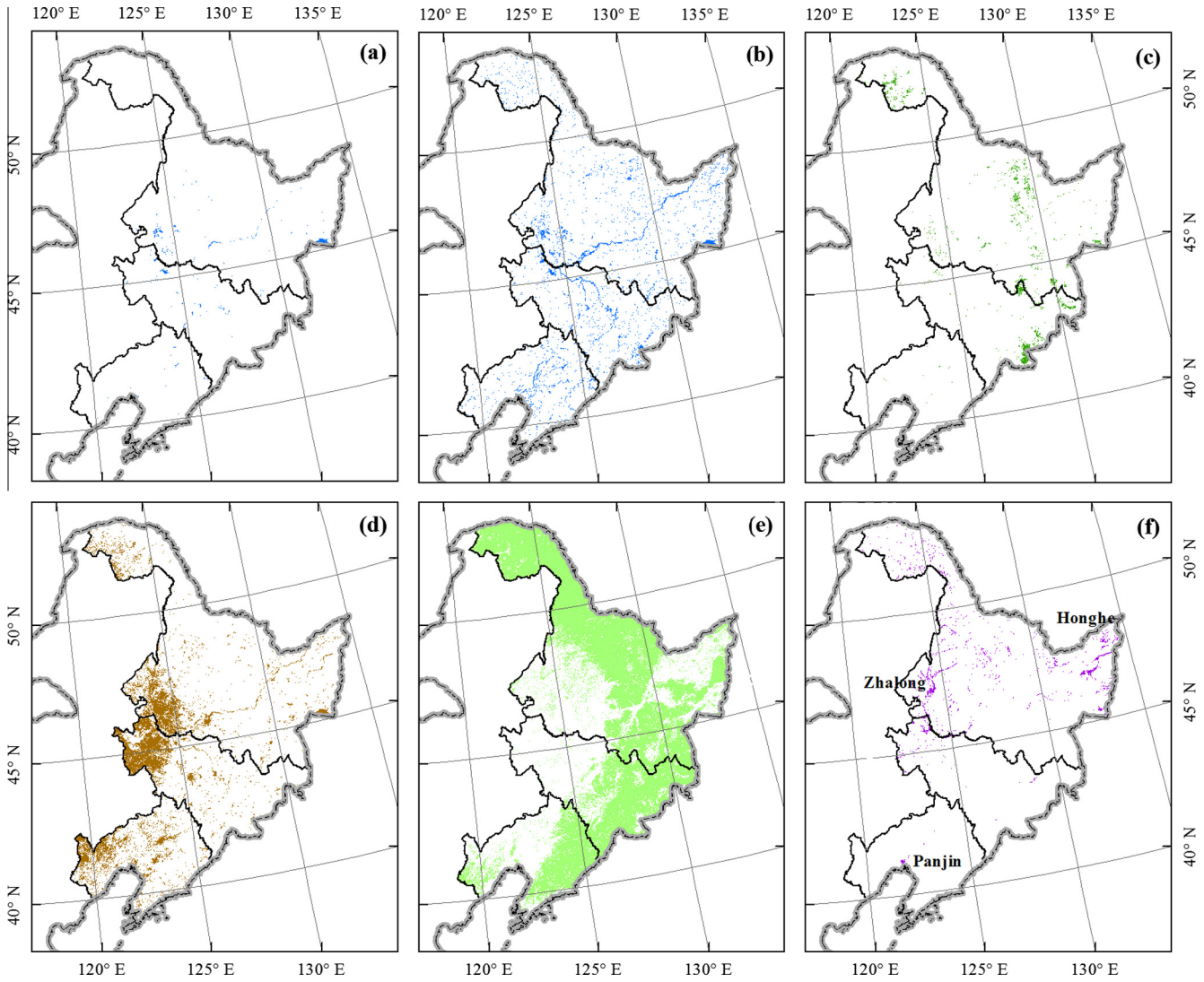

Fig. 7. Spatial distribution of (a) permanent water, (b) mixed pixels with vegetation and water bodies, (c) evergreen vegetation, (d) sparse vegetation, (e) natural deciduous vegetation with quick growth around the period of the starting date of nighttime LST remaining stable above 10 °C and NDVI > 0.4, and (f) NLCD-based natural wetland with a fraction of >= 80% in each pixel in northeastern China in 2010.

(LSWI > 0) (Fig. 3d). Here, we considered the pixels with no LSWI values of <0 in a year to be evergreen vegetation pixels (Xiao et al., 2005, 2009). One mask of evergreen vegetation was generated for each MODIS tile (Fig. 7c), and those pixels were excluded from the identification of flooding and paddy rice fields.

2.4.5. Sparse vegetation (saline and alkaline land)

Extensive areas of saline and alkaline land are distributed in the western part of the study area (Fig. S2b). We identified and mapped sparse vegetation using the annual maximum EVI data. The maximum EVI value of paddy rice is greater than 0.6 (Fig. 3a), while that of the sparse vegetation is less than 0.5 (Fig. 3e). We generated a map of sparse vegetation for the pixels with maximum EVI values of $\leqslant$0.5 (Fig. 7d). There is good spatial consistency between the NLCD-based saline and alkaline land and the pixels with maximum EVI values of less than 0.5 (Fig. S2).

2.4.6. Natural deciduous vegetation

Natural deciduous vegetation (deciduous forests, shrub, grasslands) start to become green after the nighttime LST reaches 0 °C and can have high NDVI values (>0.4) by the time the nighttime LST reaches 10 °C. In comparison, when the LST first reaches 10 °C, the paddy rice canopy is still low (NDVI < 0.4) and exhibits flooding signals (Fig. 2b). We generated a natural deciduous vegetation mask using NDVI > 0.4 for the period between LST > 0 °C and LST $\leqslant$ 10 °C after excluding the masks described above (Fig. 7e). Those pixels identified as natural deciduous vegetation were not included in the identification of flooding and paddy rice fields.

2.4.7. NLCD-based natural wetlands

The study area contains several large natural wetlands, such as the Zhalong natural wetland in western Heilongjiang Province, the Honghe natural wetland in northeastern Heilongjiang Province, and the Panjin natural wetland in southern Liaoning Province (Fig. 7f). Natural wetlands tend to grow more rapidly and flood earlier than paddy rice fields due to the spring snowmelt and increased river flow (Fig. 3f and S3). While most natural wetlands are included in the natural deciduous vegetation mask described in Section 2.4.6, we found that in some areas (such as Zhalong), natural wetlands and paddy rice have similar growth characteristics with similar flooding and canopy closure time periods (Fig. S3a). These kinds of wetlands are difficult to distinguish from paddy rice. To develop a more accurate paddy rice map, we used the natural

wetland map derived from the NLCD dataset in 2010 as a mask to exclude natural wetlands.

2.5. Validation of the MODIS-based paddy rice map using VHRI data

The accuracy of the MODIS-based paddy rice map was evaluated using validation data extracted from Google Earth Very High Resolution Imagery (VHRI). The VHRI data around 2010 were available in the Google Earth historical imagery database despite the incomplete coverage in the study area. For the samples without available VHRI, we used Landsat TM/ETM+ images as reference data. The stratified random sampling method was used to design the locations of the validation samples and we used NLCD land cover information as geographic stratification for the generation of the random samples of different land cover types. Based on the sampling points, we digitized the areas of interest (AOIs) as polygons in Google Earth by referring the VHRI, and each AOI is larger than one MODIS pixel (500 m × 500 m). We also collected more than 10,000 field photos in the study area through an intensive field survey in the summer of 2013, and all the photos were managed in the Global Geo-Referenced Field Photo Library (http://www.eomf.ou.edu/photos/, see Fig. S4 for the locations of the photos). We used selected photos for the interpretation of the VHRI and the validation data collection as they can show the crop and land use types (Dong et al., 2013, 2012). For example, paddy rice fields can be identified due to its relatively smaller field sizes and regular rectangle shapes (Fig. S5). Finally we generated 299 AOIs (2143 pixels) for paddy rice and 515 AOIs (7685 pixels) for non-paddy rice, including 96 upland crop AOIs (514 pixels), 99 forest AOIs (656 pixels), 101 built-up land AOIs (2530 pixels), 100 water body AOIs (2959 pixels), and 119 wetland AOIs (1026 pixels). The spatial distribution of the derived AOIs is shown in Fig. S5 of SI. The producer and user accuracy of paddy rice, as well as the commission and omission errors, were calculated to quantify the accuracy of the paddy rice map.

2.6. Comparison with the paddy rice data from the 2010 NLCD dataset

The NLCD dataset for China was generated by the Chinese Academy of Sciences through analyses of Landsat Thematic Mapper (TM) and Enhanced Thematic Mapper (ETM+) images acquired over five periods (1980s, 1995, 2000, 2005, and 2010) for China (Liu et al., 2014, 2005). A classification system of six primary land cover categories and 25 subtypes was used in the NLCD project, including "paddy cropland" (paddy rice) and "dry cropland" (upland crops) categories. The images were geo-referenced and orthorectified with ground control points and high-resolution digital elevation models. Visual interpretation and digitization were conducted to generate the thematic maps of land cover in China at a scale of 1:100,000. The resultant vector dataset was converted into a gridded raster at a 1-km spatial resolution, which includes area information for each land cover category. The original vector datasets are not open to the public but the 1-km gridded raster datasets are freely available through offline application. The 1-km resolution gridded "paddy rice" layer of the 2010 NLCD dataset was used to compare with the MODIS-based rice maps. According to the 2010 NLCD dataset, there was a total area of 4.6×10^4 km^2 of paddy rice and 25.3×10^4 km^2 of upland crops in the three provinces, which accounted for 6% and 32%, respectively, of the total land area in the study region (Table 1).

The scale issue needs to be considered when comparing a 500-m spatial resolution binary (0 or 1 binary set) paddy rice map derived from MODIS data (MOD_{rice}) to a fractional-area dataset derived from NLCD with a 1-km spatial resolution. In our previous study, we chose an appropriate threshold of percentage fractional cover of the reference dataset for the comparisons because the moderate resolution product could not detect pixels with small percentages of paddy rice fields (Xiao et al., 2005). The cumulative frequency distribution of the paddy rice fields based on the 2010 1-km NLCD dataset by province (Fig. 8) shows that some regions have small and fragmented paddy rice fields. The medians (50% of the pixels) for the fractions of paddy rice fields within 1-km pixels were 24% in Jilin Province and 42% in Heilongjiang Province (Table 1), which indicated that the paddy rice fields in Jilin Province were more fragmented, such as in the mountainous regions with low percentage fractions in each pixel in the south part of the province (Fig. 9a). Therefore, it is important to set a suitable threshold for the fractional coverage of NLCD-based paddy rice to evaluate the MODIS-based paddy rice map.

The definition of the minimal fractional coverage depends on the pixel size of both the NLCD-2010 and MOD_{rice}. The MODIS pixel in the MOD09A1 product has a spatial resolution of 463 m × 463 m and an area of 214,369 m^2, which accounts for 21% the area of a 1 km pixel (1,000,000 m^2) in the NLCD-2010 dataset. Thus, the pixels with a fractional coverage of $\geqslant$20% are designated as paddy rice pixels, and a binary map of paddy rice fields is generated (hereafter $NLCD_{20}$). The total area of paddy rice from all of the paddy rice pixels ($NLCD_{20}$) by calculating fractional area is approximately 43,276 km^2, which is approximately 93% of the total paddy rice area in the three provinces in northeastern China (46,471 km^2; Table 1).

We compared the MOD_{rice} map with the NLCD paddy rice layer at (1) the pixel level and (2) the administrative unit level. The paddy rice areas were calculated by using two approaches: (1) the pixel number-based paddy rice area based on MOD_{rice} and $NLCD_{20}$ which assumed that both MODIS-based paddy rice pixels and $NLCD_{20}$ paddy rice pixels have 100% fractional cover of paddy rice within the individual pixels, and (2) the fractional area-based paddy rice area based on the MOD_{rice} pixels and NLCD pixels in which rice fraction areas larger than 20%.

2.7. Comparison with the 2010 agricultural census data

The agricultural census data, which were derived from the 2010 statistical yearbooks of Heilongjiang, Jilin and Liaoning Provinces (Heilongjiang, 2011; Jilin, 2011; Liaoning, 2011), were used to compare and evaluate the MODIS-derived paddy rice maps at the prefectural level. Paddy rice planting area data are available at the province and sub-province levels in the yearbooks. There are two levels of administrative units (prefectures and counties), and the prefectures administratively oversee the counties. In Heilongjiang and Liaoning Provinces, only prefectural level data

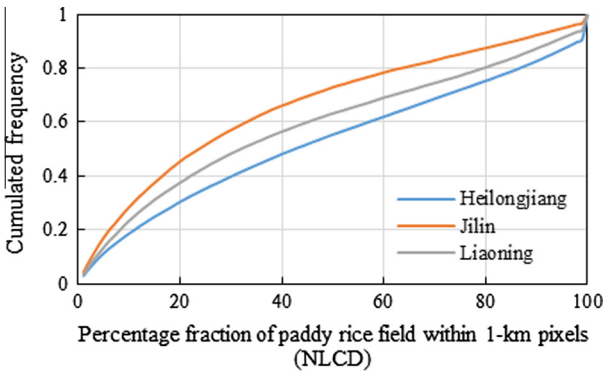

Fig. 8. Histograms of paddy rice fields within 1-km NLCD-2010 pixels by provinces in northeastern China. The cumulated frequency is used in the graph.

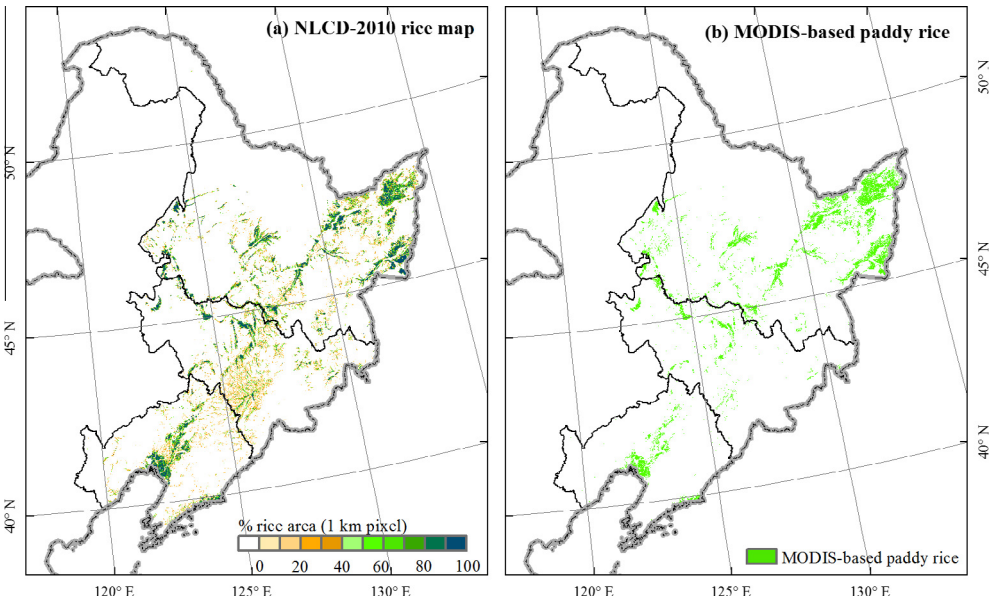

Fig. 9. Spatial distribution of paddy rice fields in northeastern China, as derived from (a) the NLCD-2010 database (Liu et al., 2014), and (b) the analysis of MODIS 8-day surface reflectance data and land surface temperature data in 2010.

were available, while county level data were available for Jilin province. There were 36 prefectures in the region (including 13 in Heilongjiang Province, 9 in Jilin Province, and 14 in Liaoning Province).

3. Results

3.1. Paddy rice map of northeastern China from MODIS data in 2010

The spatial distribution of MODIS-derived paddy rice fields in northeastern China in 2010 (MOD_{rice}) is shown in Fig. 9b. Paddy rice fields were distributed throughout the three provinces, and Heilongjiang Province had the largest area of paddy rice fields. The paddy rice fields were mainly concentrated in two major alluvial plains (the Sanjiang Plain in Heilongjiang Province and Liaohe Plain in Liaoning Province), and extensive paddy rice fields were also located along rivers, such as the Songhua River, Liao River, and Wusuli River. Most paddy rice fields were distributed in regions with elevations of less than 200 m asl with the exception of the mountainous region in the south of Jilin Province. The MODIS-derived paddy rice estimate was 39,239 km^2 in northeastern China (Table 3).

3.2. Evaluation of the MOD_{rice} map from ground truth data

The MODIS-based rice map was validated based on ground truth data, and the confusion matrix is shown in Table 2. The paddy rice map had a high producer accuracy (92%) and user accuracy (96%), while the omission and commission errors were 8% and 4%, respectively. The overall accuracy was 97%, and the Kappa coefficient was 0.92. The results indicate that the MODIS-derived paddy rice map of our study area has a high accuracy.

3.3. Comparison between the MOD_{rice} map and the NLCD-based rice layer

At the pixel level, the spatial pattern of paddy rice fields from MOD_{rice} was consistent with that of the NLCD-based paddy rice data layer, particularly for the pixels with area percentages $\geqslant$40% (Fig. 9). According to the pixel number-based comparison

Table 2
Confusion matrix of the paddy rice map accuracy assessment using areas of interest (AOIs) from the high-resolution images from 2010 in Google Earth.

Class	Ground truth pixels		Total	User accuracy
	Paddy rice	Non-paddy rice		
Paddy rice	1977	93	2070	96%
Non-paddy rice	165	7496	7661	98%
Total	2142	7589	9731	
Producer accuracy	92%	99%		

Note: overall accuracy = 97%; Kappa coefficient = 0.92.

of paddy rice area, the common paddy rice area of MOD_{rice} and $NLCD_{20}$ accounted for 72% of the MOD_{rice} area and 58% of the $NLCD_{20}$ area, respectively (Table 3). However, there were several notable differences between the MOD_{rice} map and the $NLCD_{20}$ map. First, MOD_{rice} identified more paddy rice fields than the NLCD-2010 product in the Sanjiang Plain in northeast Heilongjiang Province. Our MOD_{rice} result was verified to be correct using the Google Earth high resolution images of those regions. Second, the paddy rice planting area identified by MOD_{rice} was generally smaller than that of the NLCD dataset in the entire study area (Table 3). The inconsistencies between MOD_{rice} and $NLCD_{20}$ were concentrated in the mountainous regions, especially in Jilin

Table 3
Provincial-level comparison of area estimates of the paddy rice fields (km^2) from MODIS data in 2010 and the National Land Cover Dataset (NLCD) in 2010 (Liu et al., 2014). Two types of statistics were included: the pixel number-based area and the fractional area-based area.

Province	Pixel number-based comparison of paddy rice area (km^2) assuming a 100% fraction			Fractional area-based comparison of paddy rice area (km^2)	
	MOD_{rice}	$NLCD_{20}$	Both MOD_{rice} and $NLCD_{20}$	MOD_{rice}	$NLCD_{20}$
Heilongjiang	41,703	39,663	27,943	28,637	25,317
Jilin	7915	17,262	6154	5068	9403
Liaoning	8040	14179	7130	5534	8556
Total	57,658	71,104	41,227	39,239	43,276

Province (Fig. 9), where many pixels in the NLCD-based dataset had a fractional coverage of ⩽40% paddy rice. The MOD_{rice} may underestimate rice fields in this region because the moderate spatial resolution MODIS data cannot detect small paddy rice fields. According to the fractional area-based comparison of paddy rice area, NLCD-based results also had a higher estimate than that of MOD_{rice} (Table 3).

At the administrative level, two comparisons between the MOD_{rice} and $NLCD_{20}$ rice maps were conducted at the prefectural and county levels (36 prefectures and 182 counties, Fig. 10). The total areas of paddy rice fields of different administrative regions were calculated by overlaying administrative boundaries with the paddy rice maps.

First, we used the pixel number approach to calculate the total paddy rice area of each county and prefecture. The total area estimates of paddy rice from MOD_{rice} and $NLCD_{20}$ were significantly ($P < 0.001$) correlated (Fig. 10a and c) with a coefficient of determination (R^2) = 0.87 and a root mean square error (RMSE) = 1053 km^2 at the prefectural level ($n = 36$) and $R^2 = 0.84$ and RMSE = 268 km^2 at the county level ($n = 182$). Second, we used the fractional area approach to calculate the total paddy rice area within each county and prefecture. The fractional area-based comparison had stronger linear relationships in the area estimates of paddy rice between MOD_{rice} and $NLCD_{20}$ (Fig. 10b and d), with $R^2 = 0.90$ and RMSE = 393 km^2 at the prefectural level ($n = 36$) and $R^2 = 0.88$ and RMSE = 101 km^2 at the county level ($n = 182$). Based on the strong relationship between the two datasets at the prefectural and county levels, our MODIS-based algorithm performed well relative to the higher resolution Landsat-based results. Given the high temporal resolution, the MODIS-based algorithm could help provide timely annual rice area estimates.

3.4. Comparison with agricultural statistical data

We compared the MODIS-based paddy rice products with the statistical data at the prefectural level (Fig. 11). The R^2 between the MODIS-based data and the statistical data was 0.50; and the correlation was significant at the level of $p < 0.001$ ($n = 36$). The RMSE between them was 1444 km^2. Compared with level of the consistency between the MODIS-derived results and the NLCD data (Fig. 10), the MODIS-derived data exhibits low consistency with the agricultural census data.

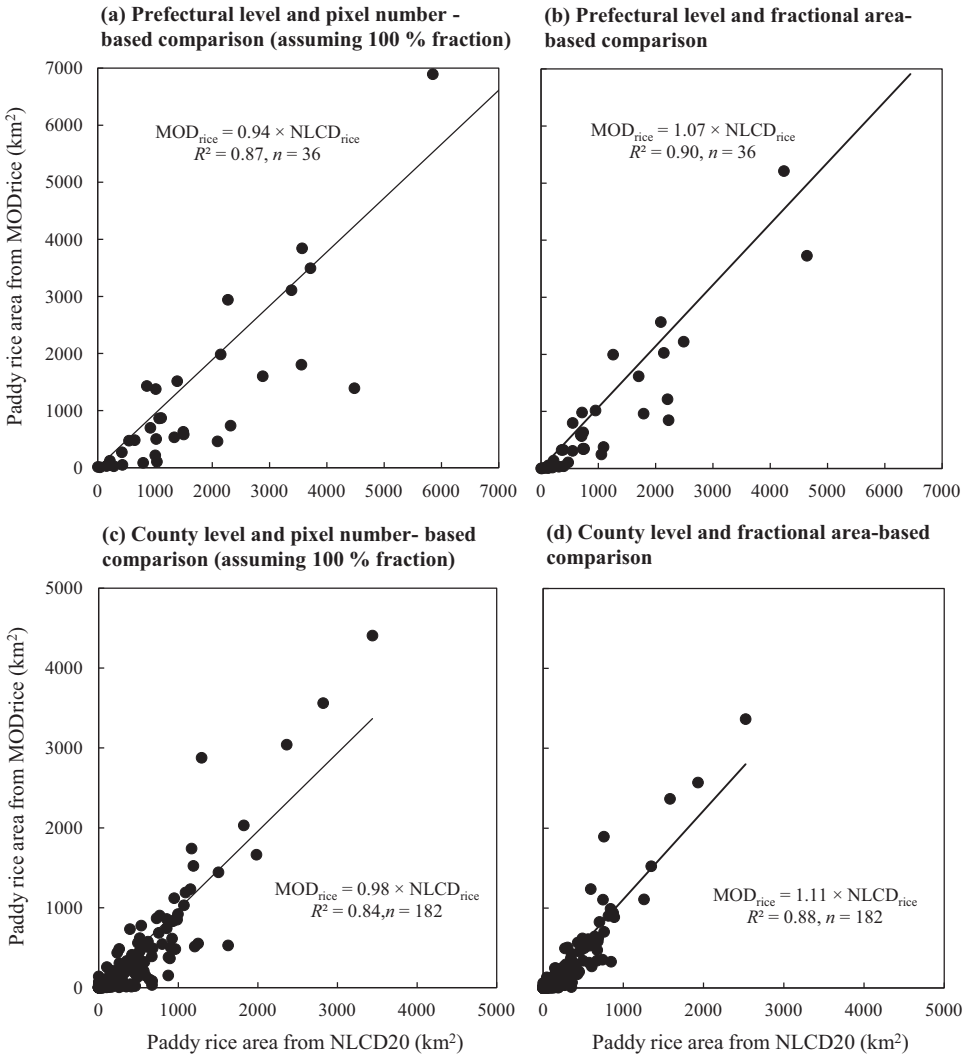

Fig. 10. The pixel number-based comparisons of paddy rice areas in northeastern China between the MODIS-based results (MOD_{rice}) and NLCD dataset ($NLCD_{20}$) at (a) the prefectural level and (c) county level; The fractional area-based comparisons of paddy rice areas in northeastern China between the MOD_{rice} and $NLCD_{20}$ at (b) the prefectural level and (d) county level. The pixel number-based comparison approach assumed that all MOD_{rice} pixels and the $NLCD_{20}$ paddy rice pixels have 100% fractional cover of paddy rice, while the fractional area-based paddy rice area based on the MOD_{rice} pixels and NLCD pixels in which rice fraction areas larger than 20%.

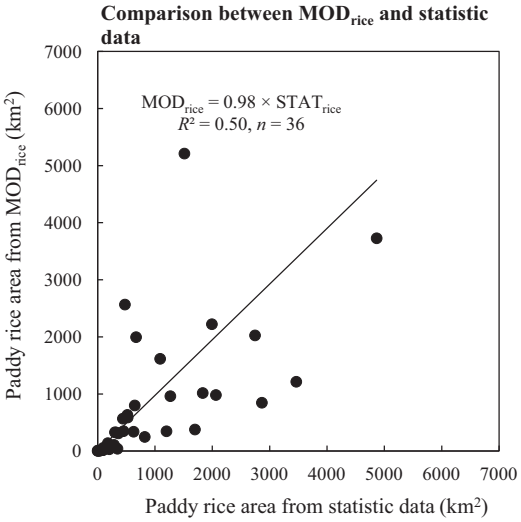

Fig. 11. Prefectural-level area comparison of paddy rice fields in northeastern China between MOD_{rice} data and statistical data.

4. Discussion

4.1. Improvement of phenology-based paddy rice algorithms

In this study, we improved the phenology-based approach for identifying paddy rice fields and applied it to generate a paddy rice map of northeastern China in 2010, where paddy rice mapping can be influenced by snowmelt in the spring. This study is an extension and improvement of our previous studies in Southeast Asia and south China (Xiao et al., 2006, 2005). The key aspect of the improved paddy rice mapping algorithm is to detect the flooding signal of paddy rice fields during suitable period for flooding and transplanting, which has not been defined clearly in previous phenology-based paddy rice mapping efforts (Peng, 2009; Peng et al., 2011; Shi et al., 2013; Sun et al., 2009; Xiao et al., 2006, 2005). This study has improvements in three areas compared to the previous studies (Table 4).

First, we improved the phenology-based algorithm by explicitly defining the suitable period for flooding and rice transplanting. In our previous studies in southern China and South and Southeastern Asia, the flooded pixels for one year were defined first and then merged as potential paddy rice fields (Xiao et al., 2006, 2005). Shi et al. (2013) and Peng et al. (2011) attempted to narrow the flooding and transplanting period and selected certain 8-day composites based on agricultural phenology observation data in northeast China and Hunan province in China, respectively. All of the pixels in those composites were considered to have the same period of flooding. For example, Shi et al. (2013) merged the flooded pixels during May and June (from approximately the 16th to 23rd 8-day MODIS composites) as the potential paddy rice regions in northeastern China based on the phenology observation data (Fig. 2c and d). The result of this method is shown in Fig. 5b, which is similar to our flooding map (Fig. 5a) but includes more disturbances from forests and other natural vegetation. Sun et al. (2009) also generated a spatial dataset of flooding and transplanting periods in China by spatial interpolation of the agricultural phenology observation data. However, the agricultural phenology observation data were limited and scattered and had bias in being used to acquire wall-to-wall phenology information. In this study, we used the spatial LST data to define the start of the flooding (SOF) of the paddy rice fields; specifically, the date after which the nighttime LST remained above 5 °C was determined to be the SOF. We also found that EVI 0.35 can be an effective indicator of the end of flooding (EOF) based on time series analysis (Figs. 2b and 3a). The suitable period for flooding and transplanting (SOF and EOF) were extracted for individual pixels. The flooding and transplanting region that was identified between SOF and EOF (Fig. 5a) closely matches the resultant paddy rice map in Fig. 9b.

Second, we simplified the flooding signal extraction process by using two indices (EVI and LSWI) instead of three (NDVI, EVI, and

Table 4
Comparison of the existing phenology-based paddy rice mapping algorithms.

Reference	Rules in phenology-based algorithms	Study area
Xiao et al. (2006, 2005)	(1) Flooding and transplanting identification: LSWI + 0.05 >= EVI or LSWI + 0.05 >= NDVI (2) Flooding and transplanting timing: all 8-day composites in one year (3) Quick growth rule: the EVI value reaches half of the maximum EVI value (in that crop cycle) within five 8-day composites following the date of flooding and transplanting	South Asia, Southeast Asia, and southern China
Sun et al. (2009)	(1) Flooding and transplanting identification: LSWI > 0.12, EVI < 0.26, and LSWI + 0.05 > EVI for single and early rice identification; LSWI > 0.12, EVI > 0.35, and LSWI + 0.17 > EVI for late rice identification (2) Flooding and transplanting timing: flooding and transplanting period according to agricultural observations (3) Quick growth rule: the average EVI of the 6th to 11th 8-day composites after transplanting was greater than 0.35	China
Shi et al. (2013)	(1) Flooding and transplanting identification: $LSWI_{2105}$ > 2EVI (2) Flooding and transplanting timing: from May to June according to agricultural observations (3) Quick growth rule: the mean EVI of the 7th to 11th 8-day composites is greater than or equal to 0.45	Northeastern China
Peng (2009), Peng et al. (2011)	(1) Flooding and transplanting identification: LSWI + T > EVI for single, early and late rice identification, and the threshold T is different for different rice types in different years (2) Flooding and transplanting timing: according to agricultural observations (3) Quick growth rule: the EVI value during rice heading period reaches 0.55	Hunan Province in China
This study	(1) Flooding and transplanting identification: LSWI + 0.05 >= EVI (2) Flooding and transplanting timing: between the date of LST 5 °C (SOF) and EVI 0.35 (EOF) (3) Quick growth rule: none	Northeastern China

LSWI). Our previous studies (Xiao et al., 2006, 2005) mathematically defined flooding as LSWI + 0.05 ⩾ EVI or LSWI + 0.05 ⩾ NDVI. Sun et al. (2009) used the condition LSWI + 0.05 > EVI and two additional conditions (LSWI > 0.12 and EVI < 0.26 during the flooding and transplanting period) to identify the "inundation signals" of the single and early rice in China. Peng (2009) and Peng et al. (2011) used a similar condition (LSWI + T > EVI) to detect paddy rice fields in Hunan Province, China, where T is the threshold, which has different values for different years and paddy rice types (single, early and late rice). These previous studies followed a similar principle as our previous studies (Xiao et al., 2006, 2005) but added more specific conditions that helped to exclude the other land cover types; however, the method is not robust and practical for large scale and long term applications. In this study, we simplified the flooding extraction equation and improved the mapping process by using more masks (i.e., persistent water, evergreen vegetation, mixed pixels with water and vegetation).

Third, the rapid growth rule was not considered in this study to further simplify the algorithm for identifying paddy rice planting areas. Rapid growth and canopy closure is an important stage that follows the flooding and transplanting of rice and can be a useful feature to extract paddy rice. Our previous studies (Xiao et al., 2006, 2005) showed that the EVI value of a rice pixel reaches half of the maximum EVI value (in that crop cycle) within five 8-day increments (approximately 40 d) after transplanting. Sun et al. (2009) assumed that the average EVI value of the 6th to 11th 8-day composites after transplanting was greater than 0.35 for a rice pixel. Shi et al. (2013) assumed that the mean EVI value of the 7th to 11th 8-d composites is greater than or equal to 0.45, and Peng (2009) and Peng et al. (2011) assumed that the EVI value reaches 0.55 during the rice heading period. These studies applied different thresholds for different stages around the rapid growth stage; thus, the approach is difficult to extend to a larger scale. The temporal profile analysis in Fig. 3 shows that a threshold in the rapid growth stage may have a limited effect because forests and natural wetlands can meet the requirement as well. Flooding and transplanting is the most unique characteristic of paddy rice. Fig. 5a shows that the flooding and transplanting area between SOF and EOF is similar to the final paddy rice map with only limited commission errors from natural wetlands, dryland crops, and forests, which also meet the conditions of the rapid growth stage. We argue that the identification of the flooding and transplanting signals in the early phases of the paddy rice calendar are sufficient to extract the paddy rice planting area given that multiple masks are used in this study.

4.2. Comparison between the MODIS- and phenology-based approach and landsat- and visual interpretation approach

Although the spatial distribution of paddy rice from MOD_{rice} agrees well with the spatial pattern from $NLCD_{20}$, there are several regional differences, especially in Jilin and Liaoning Provinces. The reasons for the discrepancies between the MOD_{rice} and $NLCD_{20}$ area estimates are complex.

First, due to the moderate resolution of the MODIS data (500 m), our algorithm could not identify paddy rice fields in the regions where the areas of paddy rice fields are much smaller than a MODIS pixel; this was also mentioned in previous studies (Peng et al., 2011; Shi et al., 2013; Sun et al., 2009; Xiao et al., 2006, 2005). For example, paddy rice fields in the southern part of Jilin Province were mainly distributed in the mountainous regions according to the NLCD dataset, and area percentages of paddy rice were less than 40% in the 1-km pixels. It is difficult for MODIS data to identify paddy rice fields in fragmented mountainous areas, which could have led to underestimations of MODIS-based paddy rice fields. Several challenges arise when assessing the accuracy of moderate-resolution (500 m) land cover products, as the MODIS-based maps can overestimate or underestimate area of individual land cover types due to the fragmentation and sub-pixel proportions of the individual land cover types. Alternative strategies include temporal mixture analysis (Yang et al., 2012) and the hierarchical training technique (Jain et al., 2013).

Second, there are several uncertainties in the NLCD dataset. The NLCD products were generated by using one Landsat image during the growing season instead of multi-temporal images. The image used substantially affects visual interpretation capability because the paddy rice and other crops (wheat, corn) have similar spectral signatures at the peak of the growing season. For example, several paddy rice fields were identified from NLCD data in the area of Dunhua city in Jilin Province, but only a few were identified from the MODIS data. We randomly extracted four samples from the NLCD-based paddy rice region in this area and plotted the curves of the MODIS vegetation indices from 2008 to 2012 (Fig. S6). We found that there were no flooding/transplanting signals in those samples during this period, which indicated that the sample regions were not paddy rice fields. Additionally, we compared the area of paddy rice fields in Dunhua from the NLCD dataset in 2010 with data from the 2010 statistical yearbook of Jilin Province (Jilin, 2011). The areas of paddy rice fields in Dunhua were 352 km^2 from the NLCD dataset but only 52 km^2 from the statistical yearbook, which further indicates that there is some bias toward NLCD-based paddy rice fields in Dunhua. Therefore, using MODIS time series data to identify crops has several advantages over visual interpretation of Landsat images in the NLCD dataset.

Third, paddy rice and some natural wetlands in the study area have similar phenology characteristics (Fig. S3), thus, it is difficult to distinguish paddy rice from natural wetlands using the phenology-based approach. We excluded some natural wetlands using NDVI > 0.4 during the period of LST over 10 °C. Shi et al. (2013) identified natural wetlands and forests based on the rules NDVI > 0.4 and $NDVI\text{-}LSWI_{2105} > 0.05$ over 15 8-day composites during the year based on the long growing season of natural wetland and forest from mid-late April to mid-October. However, some wetlands cannot be excluded because of the similar features of paddy rice and natural wetlands in some regions, which could lead to overestimating the area of paddy rice fields (Fig. S3). In this situation, shape and size information can be useful for extracting natural wetlands by visual interpretation. We masked those natural wetlands based on the NLCD dataset. However, there is still a need to develop a MODIS-based natural wetland mask in the future, which will help to develop a uniform MODIS-based paddy rice mapping protocol.

When we compared MOD_{rice} with the statistical agricultural data (Fig. 11), the consistency between them was significantly lower than between MOD_{rice} and $NLCD_{rice}$ (Fig. 10b). The primary reason can be attributed to the quality of the statistical data provided by China's State Statistical Bureau (SSB). Statistical data in China can be biased due to political and policy factors (Crook, 1993; Deng et al., 2006; Frolking et al., 1999; Liu et al., 2005; Seto et al., 2000; Xiao et al., 2003a). Xiao et al. (2003a) showed that the cropland area in China from official agricultural census was underestimated by comparisons with different cropland areas data. The SSB also reported that cultivated areas were underestimated in China (State Statistical Bureau, 1994). The consistency between $NLCD_{rice}$ and MOD_{rice} indicates the reliability of the MODIS-based paddy rice map developed in this study.

5. Conclusions

Many studies have reported on paddy rice distribution in sub-tropical and tropical regions, but paddy rice in temperate and cold temperate zones has received little attention. This study extended our previous efforts in mapping paddy rice in southern China, Southeastern Asia, and South Asia into northern monsoon Asia. This is the first study to demonstrate the potential of MODIS LST data and vegetation index data in mapping paddy rice planting areas. We improved the phenology-based algorithm by accurately defining the temporal window of flooding and transplanting based on MODIS LST data. The resultant paddy/non-paddy rice map had an overall accuracy of 97% and Kappa coefficient of 0.92 based on the validation data derived from the Google Earth VHRI data and the field photos. The results from this study also demonstrated that our improved algorithm is simple and robust and can be used to map paddy rice plant areas in other temperate and cold temperate zones, including Japan and the Korean Peninsula. Together with our previous efforts (Xiao et al., 2005, 2006), our long-term goal is to use a consistent algorithm and MODIS data to develop a database of paddy rice agriculture in monsoon Asia, which accounts for 90% of the global rice production. In addition, the area changes in paddy rice can be quantified using multi-year MODIS data since 2000, which will enable us to study the effects of climate change and human activities on the paddy rice planting area and the likely impacts of the area changes of paddy rice on the agroecosystem, biogeochemical cycles and food security.

Acknowledgements

This study was supported in part by research Grants from the NASA Land Use and Land Cover Change program (NNX11AJ35G, NNX14AD78G) and the National Institutes of Health (NIH) NIAID (1R01AI101028-01A1). We thank Melissa Scott and Sarah L. Xiao for their comments and English editing in the earlier versions of the manuscript.

Appendix A. Supplementary material

Supplementary data associated with this article can be found, in the online version, at http://dx.doi.org/10.1016/j.isprsjprs.2015.05.011.

References

Bouman, B., 2009. How much water does rice use. Rice Today 8, 28–29.
Bouvet, A. et al., 2009. Monitoring of the rice cropping system in the Mekong delta using ENVISAT/ASAR dual polarization data. IEEE Trans. Geosci. Remote Sens. 47, 517–526.
Chen, C.F. et al., 2012. Monitoring of rice cropping intensity in the upper Mekong Delta, Vietnam using time-series MODIS data. Adv. Space Res. 49, 292–301.
Crook, F.W., 1993. Underreporting of China's cultivated land area: implications for world agricultural trade. China Int. Agric. Trade Rep., 33–39
Deng, X. et al., 2006. Cultivated land conversion and potential agricultural productivity in China. Land Use Pol. 23, 372–384.
Dong, J. et al., 2013. Mapping deciduous rubber plantations through integration of PALSAR and multi-temporal Landsat imagery. Remote Sens. Environ. 134, 392–402.
Dong, J. et al., 2012. A comparison of forest cover maps in Mainland Southeast Asia from multiple sources: PALSAR, MERIS, MODIS and FRA. Remote Sens. Environ. 127, 60–73.
Dong, Y.F. et al., 2006. Monitoring of rice crop using ENVISAT ASAR data. Sci. China Ser. D-Earth Sci. 49, 755–763.
Ehhalt, D. et al., 2001. Atmospheric Chemistry and Greenhouse Gases. Pacific Northwest National Laboratory (PNNL), Richland, WA, US.
FAOSTAT, 2010. Statistical Database of the Food and Agricultural Organization of the United Nations.
Frolking, S. et al., 1999. Agricultural land-use in China: a comparison of area estimates from ground-based census and satellite-borne remote sensing. Global Ecol. Biogeogr. 8, 407–416.
Gilbert, M. et al., 2014. Predicting the risk of avian influenza A H7N9 infection in live-poultry markets across Asia. Nat. Commun. 5.
Gilbert, M. et al., 2008. Mapping H5N1 highly pathogenic avian influenza risk in Southeast Asia. Proc. Nat. Acad. Sci. U.S.A. 105, 4769–4774.
Gumma, M.K. et al., 2011. Mapping rice areas of South Asia using MODIS multitemporal data. J. Appl. Remote Sens. 5, 053547.
Hall, D.K. et al., 1995. Development of methods for mapping global snow cover using moderate resolution imaging spectroradiometer data. Remote Sens. Environ. 54, 127–140.
Hall, D.K. et al., 2002. MODIS snow-cover products. Remote Sens. Environ. 83, 181–194.
Heilongjiang, S.B.i., 2011. Heilongjiang Statistical Yearbook in 2011. China Statistics Press.
Huete, A. et al., 2002. Overview of the radiometric and biophysical performance of the MODIS vegetation indices. Remote Sens. Environ. 83, 195–213.
Huete, A.R. et al., 1997. A comparison of vegetation indices global set of TM images for EOS-MODIS. Remote Sens. Environ. 59, 440–451.
Jain, M. et al., 2013. Mapping cropping intensity of smallholder farms: a comparison of methods using multiple sensors. Remote Sens. Environ. 134, 210–223.
Jilin, S.B.i., 2011. Jilin Statistical Yearbook in 2011. China Statistics Press.
Kamthonkiat, D. et al., 2005. Discrimination of irrigated and rainfed rice in a tropical agricultural system using SPOT VEGETATION NDVI and rainfall data. Int. J. Remote Sens. 26, 2527–2547.
Kuenzer, C., Knauer, K., 2013. Remote sensing of rice crop areas. Int. J. Remote Sens. 34, 2101–2139.
LeToan, T. et al., 1997. Rice crop mapping and monitoring using ERS-1 data based on experiment and modeling results. IEEE Trans. Geosci. Remote Sens. 35, 41–56.
Li, P. et al., 2012. Changes in rice cropping systems in the Poyang Lake Region, China during 2004–2010. J. Geogr. Sci. 22, 653–668.
Liaoning, S.B.i., 2011. Liaoning Statistical Yearbook in 2011. China Statistics Press.
Linderholm, H.W. et al., 2008. Twentieth-century trends in the thermal growing season in the Greater Baltic Area. Climatic Change 87, 405–419.
Liu, J. et al., 2014. Spatiotemporal characteristics, patterns, and causes of land-use changes in China since the late 1980s. J. Geogr. Sci. 24, 195–210.
Liu, J. et al., 2005. Spatial and temporal patterns of China's cropland during 1990–2000: an analysis based on Landsat TM data. Remote Sens. Environ. 98, 442–456.
Liu, Z. et al., 2013. Change analysis of rice area and production in China during the past three decades. J. Geogr. Sci. 23, 1005–1018.
Maclean, J.L., Hettel, G.P., 2002. Rice Almanac: Source Book for the Most Important Economic Activity on Earth. International Rice Research Institute.
Maki, M. et al., 2004. Estimation of leaf water status to monitor the risk of forest fires by using remotely sensed data. Remote Sens. Environ. 90, 441–450.
Miyaoka, K. et al., 2013. Rice-planted area mapping using small sets of multi-temporal SAR data. IEEE Geosci. Remote Sens. Lett., 1–5
Nuarsa, I.W. et al., 2012. Using variance analysis of multitemporal MODIS images for rice field mapping in Bali Province, Indonesia. Int. J. Remote Sens. 33, 5402–5417.
Pan, Z. et al., 2015. Mapping crop phenology using NDVI time-series derived from HJ-1 A/B data. Int. J. Appl. Earth Observation Geoinformation 34, 188–197.
Peng, D., 2009. The Study on the Method of Rice Yield Estimation Using Statistical and MODIS Data. Zhejiang University, Hangzhou.
Peng, D.L. et al., 2011. Detection and estimation of mixed paddy rice cropping patterns with MODIS data. Int. J. Appl. Earth Observation Geoinformation 13, 13–23.
Samad, M. et al., 1992. Irrigation management strategies for improving the performance of irrigated agriculture. Outlook Agric. 21, 279–286.
Sass, R.L., Cicerone, R.J., 2002. Photosynthate allocations in rice plants: food production or atmospheric methane? Proc. Nat. Acad. Sci. U.S.A. 99, 11993–11995.
Sass, R.L. et al., 1999. Exchange of methane from rice fields: national, regional, and global budgets. J. Geophys. Res. Atmos. 104, 26943–26951.
Seto, K.C. et al., 2000. Landsat reveals China's farmland reserves, but they're vanishing fast. Nature 406, 121-121.
Shi, J.J. et al., 2013. Multi-year monitoring of paddy rice planting area in Northeast China using MODIS time series data. J. Zhejiang Univ. Sci. B 14, 934–946.
Son, N.-T. et al., 2013. A phenology-based classification of time-series MODIS data for rice crop monitoring in Mekong Delta, Vietnam. Remote Sens. 6, 135–156.
State Statistical Bureau, S., 1994. Statitical Yearbook of China 1994. China Statistical Publishers House, Beijing.
Sun, H. et al., 2009. Mapping paddy rice with multi-date moderate-resolution imaging spectroradiometer (MODIS) data in China. J. Zhejiang Univ. Sci. A 10, 1509–1522.
Thi, T.H.N. et al., 2012. Mapping the irrigated rice cropping patterns of the Mekong delta, Vietnam, through hyper-temporal SPOT NDVI image analysis. Int. J. Remote Sens. 33, 415–434.
Vermote, E., Vermeulen, A., 1999. Atmospheric correction algorithm: spectral reflectances (MOD09). ATBD version 4.
Wan, Z.M., 2008. New refinements and validation of the MODIS land-surface temperature/emissivity products. Remote Sens. Environ. 112, 59–74.
Wan, Z.M. et al., 2002. Validation of the land-surface temperature products retrieved from Terra moderate resolution imaging spectroradiometer data. Remote Sens. Environ. 83, 163–180.
Wu, F. et al., 2011. Rice crop monitoring in south china with RADARSAT-2 quad-polarization SAR data. IEEE Geosci. Remote Sens. Lett. 8, 196–200.
Xiao, X. et al., 2006. Mapping paddy rice agriculture in South and Southeast Asia using multi-temporal MODIS images. Remote Sens. Environ. 100, 95–113.

Xiao, X. et al., 2002a. Landscape-scale characterization of cropland in China using vegetation and landsat TM images. Int. J. Remote Sens. 23, 3579–3594.
Xiao, X. et al., 2002b. Observation of flooding and rice transplanting of paddy rice fields at the site to landscape scales in China using vegetation sensor data. Int. J. Remote Sens. 23, 3009–3022.
Xiao, X. et al., 2005. Mapping paddy rice agriculture in southern China using multi-temporal MODIS images. Remote Sens. Environ. 95, 480–492.
Xiao, X. et al., 2002c. Quantitative relationships between field-measured leaf area index and vegetation index derived from VEGETATION images for paddy rice fields. Int. J. Remote Sens. 23, 3595–3604.
Xiao, X. et al., 2003a. Uncertainties in estimates of cropland area in China: a comparison between an AVHRR-derived dataset and a Landsat TM-derived dataset. Global Planet. Change 37, 297–306.
Xiao, X.M. et al., 2009. A simple algorithm for large-scale mapping of evergreen forests in tropical America, Africa and Asia. Remote Sens. 1, 355–374.
Xiao, X.M. et al., 2003b. Sensitivity of vegetation indices to atmospheric aerosols: continental-scale observations in Northern Asia. Remote Sens. Environ. 84, 385–392.
Yang, F. et al., 2012. Temporal mixture analysis for estimating impervious surface area from multi-temporal MODIS NDVI data in Japan. ISPRS J. Photogrammetry Remote Sens. 72, 90–98.
Yang, S.B. et al., 2008. Rice mapping and monitoring using ENVISAT ASAR data. IEEE Geosci. Remote Sens. Lett. 5, 108–112.
Yoshikawa, N., Shiozawa, S., 2006. Estimating variable acreage of cultivated paddy fields from preceding precipitation in a tropical watershed utilizing Landsat TM/ETM. Agric. Water Manage. 85, 296–304.